Reduced FV Modelling Based on CFD Database and Experimental Validation for the Thermo-fluid Dynamic Simulation of Flue Gases in Horizontal Fire-Tubes

Alessandro Morelli [1a], Marco Tognoli[b], Antonio Ghidoni[a], Behzad Najafi[b], Fabio Rinaldi[b]

[a]*Dipartimento di Ingegneria Meccanica e Industriale, Università degli Studi di Brescia, Via Branze 38, Brescia 25123, Italy*
[b]*Dipartimento di Energia, Politecnico di Milano, Via Lambruschini 4, Milano 20156, Italy*

Abstract

The present work aims at proposing an optimized physical heat transfer correlation in smooth horizontal fire-tubes (applying a one-dimensional reduced Finite Volume Method - FVM), validated over a wide range of operating conditions. An experimental activity is first carried out, in which the temperature and pressure profiles of the flue gases, streaming through pipes while applying hot-water-boiler conditions, are measured. A Computational Fluid Dynamics (CFD) set-up is developed for simulating the thermo-physical behaviour of the flue gases undergoing a wide range of operating conditions (replicating the conditions that these streams experience in the most common industrial boiler applications). The acquired experimental data with a detailed uncertainty analysis are employed for validating the developed CFD results. Subsequently, the reduced one-dimensional FVM physical models for estimating the heat transfer (taking into account the convective and radiative terms) and pressure drops are implemented. The most accurate models are calibrated using the results of the fluid-dynamics simulations. In this procedure, the coefficients of the standard models are optimized, employing a Multi Objective Genetic Algorithm optimization procedure (MOGA). This work demonstrates that the CFD simulations can reproduce the experimental data accurately. Furthermore, the estimations of the FVM model based on the calibrated physical correlations are in good agreement with numerical results, but with a reduced computational cost. Results indicate an improved estimation of tubes outlet temperature with respect to standard correlation (42.4% error reduction), while the estimated outlet pressure shows only a slight increase of the error with respect to the Fang correlation.

Keywords: Fire-tube Boilers, Head-losses modelling, Heat Exchange Modelling, Computational Fluid Dynamics, Genetic Algorithm, Optimization

---

[1]Correspondence: a.morelli005@unibs.it

Nomenclature

A	heat exchange surface	m^2
$A2$	fuel dependent constants (for Natural Gas equal to 0.66)	
B	fuel dependent constants (for Natural Gas equal to 0.009)	
c_P	isobaric specific heat coefficient	$\frac{J}{kgK}$
c_V	isocoric specific heat coefficient	$\frac{J}{kgK}$
CFD	computational fluid dynamic	
D	euclidean distance	
d	diameter	m
DO	discrete ordinates model	
e	air excess value	$m_{air,actual}/m_{air,stoch.}$
EGR	exhaust gas recirculation	
f	friction factor	
$\vec{g}$	gravity acceleration	m/s^2
g_g	equivalent radiative resistance term	W/m^2K^4
Gr	Grashof number	
h	specific enthalpy	J/kg
h_{conv}	convective heat transfer coefficient	J/m^2K
HWB	hot water boiler	
k	kinetic energy	
L	tube length	m
LHV	fuel mass lower heating value	J/kg

m	mass	kg
$\dot{m}$	mass flow rate	kg/s
$\overline{m}$	hourly mass flow rate	kg/h
MM	molar mass	g/mol
N	number of finite volumes	
Nu	Nusselt number	
P	pressure	Pa
p	pareto	
Pr	Prandtl number	
$\dot{Q}$	heat transfer rate	kW_t
R	radius	m
R_0	universal gas constant	$J/molK$
Re	Reynolds number	
res	Element resolution	$m/element$
Ri	Richardson number	
S	average radiative path length	m
SST	shear stress transport	
T	temperature	K
t	time	s
u	measurement uncertainty	
V	volume	m^3
v	velocity	m/s
$\dot{V}$	volumetric flow rate	Nm^3/h

Greek

Δ	Difference	
η	first law efficiency term	

λ	linear thermal conductivity	W/mK
μ	Dynamic viscosity	$Pa \cdot s$
ν	specific volume	m^3/kg
ω	specific turbulence dissipation rate	
ρ	density	kg/m^3
σ	Stefan-Boltzmann's constant	
ε	emissivity	
ϑ	heat exchange efficiency	

Subscripts

∞	bulk flow conditions
abs	absolute
air	air
amb	ambient conditions surrounding the boiler
atm	atmosphere
avg	spatial average
cc	combustion chamber
$cons$	consumed quantity in a chemical process
$conv$	convective
d	Darcy
el	volume element
exp	experimental
fg	flue gas
$fuel$	fuel
gen	products generated in a chemical process
hyd	hydraulic
i	index of finite volume element

in inlet

int interior

lit literature

out outlet

rad radiative

real real

s simulation

st stoichiometric

steam steam

t thermocouple

tot total

tube tube

vessel vessel

wall inner tube wall side

1. Introduction

Fire-tube boilers are commonly used in many industrial fields and their notable energy consumption and emissions are accordingly a matter of concern. Thus, motivated by the increasingly stringent emission regulations and about the energy efficiencies of appliances, the thermal design improvement of this type of boilers components has received increasing attention. Through the analysis of the consumption share of major industrial processes, a notable portion of the global energy demand can be attributed to steam production [1]. Therefore, any marginal improvement in the boilers' energy efficiency can lead to a significant primary energy saving and fuel costs reduction and, consequently, a decrement in the corresponding emissions.

In this context, Barma et al. [1] performed a systematic investigation on boilers' performance and demonstrated that the hot flue gases' discharge at the chimney is the primary source of energy losses in the system. Furthermore, an improvement in the heat transfer efficiency, leading to the reduction of the latter loss term, has a significant potential for reducing the boilers' fuel cost over its lifespan; therefore, a more accurate development on the heat transfer surfaces is a viable solution to mitigate the aforementioned stack losses, while distributed pressure drops, caused by the flue-gas motion with respect to stationary tubes' walls, should also be accounted since a considerable energy consumption is attributed to the blower's fan [2]. The assessment of fire-tube boiler's performance requires the simulation of heat transfer mechanisms and pressure drops (occurring along the tube axis of horizontal fire-tubes), that in-turn necessitates a detailed thermal behaviour and pressure drop modeling.

Several modelling strategies have been employed in literature, based on computational fluid dynamic and on dynamic modelling combined with a discretization approach at the flue-gas side. The CFD approach has been used to investigate the heat exchange in smooth tubes employing experimental setups [3, 4]. However, these studies are conducted in a limited range of operating conditions, and the heat exchange takes place between air or exhaust gas and a liquid [5]. Numerical investigations have been conducted also on finned fire-tubes or tubes equipped with turbolators in the presence of petrol and diesel exhaust flue-gases [6–8]. These works provide accurate empirical correlations [9] for the estimation of the Nusselt number and the friction factor based on the geometrical dimensions, but few analyses have been focused on the modelling behaviour in smooth pipes [10]. Furthermore, the previous studies neglect the thermal radiation component for the low temperature at gas-side. Other studies have investigated the hot methane exhaust gases' heat exchange considering the temperature of flue gases up to $1170K$ in different scenarios. These works are focused on the presence of a flame within the energy production systems, such as industrial furnaces [11–14] and radiant boilers [15], [16], which are characterized by different characteristic dimensions and smoke chemical compositions with respect to natural-gas fed fire-tube boilers.

A dynamic modelling methodology combined with a discretization approach at the flue-gas side [17] has been also used to assess the thermal behaviour of fire-tube boilers components. Abene et. al. [18] proposed a dynamic thermal model for cold start-up phases of a 3-pass fire-tube boiler, which has been experimentally validated, introducing separate control volumes at flue-gas side for each section. In this study, separate convective and heat transfer mechanisms between the flue bulk flow side and the tube walls were implemented and validated; however, the fluid-dynamic losses were not taken into account. Finally, the authors reported a reasonable agreement between the estimated temperature data at the outlet of each control volume and the experimental data. Although the approach used by Abene et al. and by other authors in this area [19, 20] allows accurate thermal behaviour simulations, it does not provide a dimensional description of flue gas temperature and heat transfer rate along the main fire-tube axis.

A simplified FVM approach has been first employed by Gutiérrez Ortiz [21] and later revised by Tognoli et al. [17, 22] to dynamically estimate the heat transfer from each cylindrical shaped flue-gas discrete volume towards the metal walls. The mentioned model describes the internal convective heat transfer mechanism through a Dittus-Boelter equation in the turbulent flow regime, while the considered radiative mechanism describes the flame radial flux employing a gray gas model, where the emissivity is estimated by Hottel-Sarofim model [23] and pure gray Lambertian walls. Finally, in this study the authors performed a tuning procedure for convective heat transfer equations to simulate the flue gas behaviour in the gas passes, employing the experimental data. It is worth noticing that, although a detailed physical modelling approach was used in this study, no radiative heat exchange mechanism, occurring between the hot flue gases and the surrounding walls, was included.

The mentioned works were focused on dynamic estimation of the heat transfer and the thermal performances of fire-tube boilers, but equivalent steady-state energy balances can be obtained starting from the mentioned investigations.

Various studies have separately investigated different phenomena taking place in the flue gas pipes of fire-tube boilers, including the convective and radiative heat transfer mechanisms along with the corresponding pressure drop. Regarding the convective heat transfer mechanism, Taler [24] reviewed the power type correlations estimating the Nusselt number for turbulent flow of circular tubes in a wide range of Reynolds and Prandtl numbers. In this study, starting from the general Dittus-Boelter [25] equation, a set of convective heat transfer correlations were reviewed and the estimations obtained using each equation were compared with the experimental data. The author demonstrated that available simple power law correlations can provide an acceptable accuracy for the estimation of convective heat transfer mechanism within the considered range of geometrical parameters, compared with more detailed Gnielinski [26, 27] relationship.

As observed in the study by Beyne et al. [28], the radiative heat transfer from the hot combustion gaseous products represents a significant share of the global heat transfer. In this study, the authors developed a steady-state model of a traditional fire-tube boiler based on the ε-NTU methodology and separate control volumes. As the radiative heat transfer mechanism was taken into account in this investigation, a more accurate estimation of flue gas temperature was obtained. The authors employed the Taylor and Forest [29] approach for estimating the flue gas emissivity between 1200 K and 2400 K and the Talmor [30] correlation when the temperature exceeds this range. In the present study, the measured maximum flue gas temperature is below 1400 K; water vapour and carbon dioxide emissivity correlations are investigated for the relevant magnitude of the spectral emissivities of the considered gaseous species. Lallemant et al. [31] reviewed 9 different total emissivity models for $H_2O - CO_2$ gas species. The authors indicate a higher agreement with experimental data when employing Smith, Shen and Friedman [32] gray gas based model in comparison with the polynomial models and single line weighted sum gray gas models. The model proposed in the latter study, where the values are determined as a weighted summation of coefficients, is a valid option for the application that is investigated in the present study, taking into account the corresponding temperature range, the average path length and the considered nearly atmospheric pressure.

Finally, detailed models need to simulate the distributed friction losses that result from the interaction of the considerable flue-gas flow rate in tubes in presence of a fully developed turbulent flow occurring along the smooth tube's axis. Several authors approximated the Colebrook-White [33] friction factor formula in order to propose explicit solutions. These correlations, which have been reviewed in [34–36], have demonstrated to provide accurate predictions when compared to the reference Colebrook-White formula. Fang et al. [37] recently proposed two new explicit correlations for single-phase turbulent flow in pipes, the first for smooth tubes, while the second one is valid either for smooth tubes and in presence of rough tubes. The authors compared the estimations with Nikuradse [38] and Colebrook equations and showed marginal errors for a wide range of Reynolds number. It also worth noticing that the Fang correlation is compatible with the observed operating conditions investigated in the present work.

No previous work has simultaneously investigated the convective and radiative heat transfer mechanisms and the pressure drop in the flue gas pipes of fire-tube boilers in a comprehensive manner. Motivated by this research gap, the objective of this work is twofold: *i*) implementing a 1D finite volume method (FVM) based model for simulating the flow field in horizontal fire-tubes, and *ii*) providing optimized correlations for the heat transfer (convective+radiative) and pressure loss estimation (utilized in the latter FVM model). The second aim is achieved through performing an optimization procedure employing a large dataset, which is obtained using the described 3D CFD simulations, which are in turn validated utilizing the experimental data. The different activities proposed in this work and their connection are summarized in Fig. 1. A comprehensive CFD model has been first developed to simulate the aforementioned heat transfer and fluid-dynamic behaviour. The CFD model was validated with experimental investigation by Bisetto [20], which is similar to the scenario analysed in the present study and it is characterized by a similar flue-gases chemical composition. To extend the model's validity to a wide range of fire-tube configurations and operating conditions, a second validation was performed with the data obtained in an experimental activity performed on a Hot Water Boiler (HWB) at ICI Caldaie SpA laboratories [39] (an Italian manufacturing company partner of this research activity). In the next step, a revised version of Gutiérrez Ortiz [21] Finite Volume Methodology (FVM) for gas-passes side is employed in order to develop a separate detailed physical model. Subsequently, a comparative analysis among the available physical based convective heat transfer equations and friction factor correlations (considering a steady-state regime) is performed, using CFD simulations as a validation data-set, to determine the resulting temperature and pressure estimation bias. Finally, an optimization procedure, based on the Multi-Object-Genetic-Algorithm (MOGA) [40, 41] is performed to provide calibrated convective and friction factor correlations.

It is worth mentioning that once the FVM model is implemented and the utilized correlation is optimized, the optimized model can be employed to simulate the behaviour of the flue gases in other operating conditions; thus, performing computationally expensive CFD simulations will then be avoided. The latter advantage is the key benefit of employing the approach that has been utilized in the present study.

2. Experimental set-up

A fire-tube is a horizontal cylindrical pipe that separates hot flue-gases (streaming inside the pipe) from the surrounding medium, while permitting a considerable heat flux across the metal wall. It is commonly employed in fire-tube boilers in order to heat up sub-cooled/saturated water or a heat transfer medium such as diathermic oil. Furthermore, despite the considerable temperature gradient observed at the flue-gas side, a homogeneous temperature distribution is assumed for the external surface tube. The experimental measurements aim to investigate the heat transfer through tube walls and the flue-gas side's fluid dynamic losses, while the heat transfer for the water side is neglected. In the present

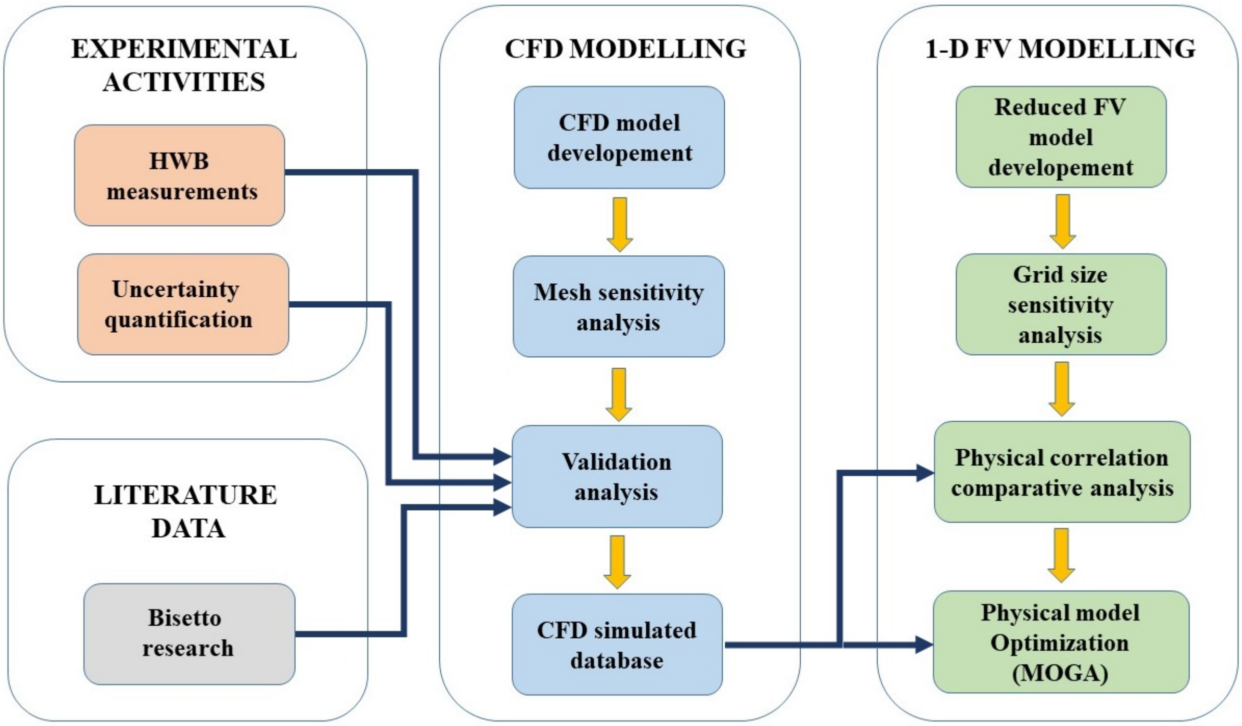

Figure 1: Research activity chart

section, details of the experimental activity (performed at ICI Caldaie SpA's laboratory) and the results used to validate the CFD model are provided.

2.1. Test-case description

The test case is based on a modified fire-tube boiler supplying hot-water at a designed temperature up to 353 K. The experimental activity has been performed on a 60 kW two-pass fire Hot-Water Boiler (HWB), which is schematically described in Fig.2, and its dimensions are reported in Table 1, to measure the heat exchange between flue gases and water. The combustion system consists of a coaxial blown burner, located inside the combustion chamber, which receives a mixture of natural gas and air from a centrifugal fan. The natural gas is supplied at a positive pressure between $20-50$ $mbar$ through a pneumatic

Parameter	Value [mm]
d_{vessel}	590
d_{cc}	390
L_{cc}	580
d_{tube}	41.3
L_{tube}	620

Table 1: The geometrical characteristics of the considered HWB

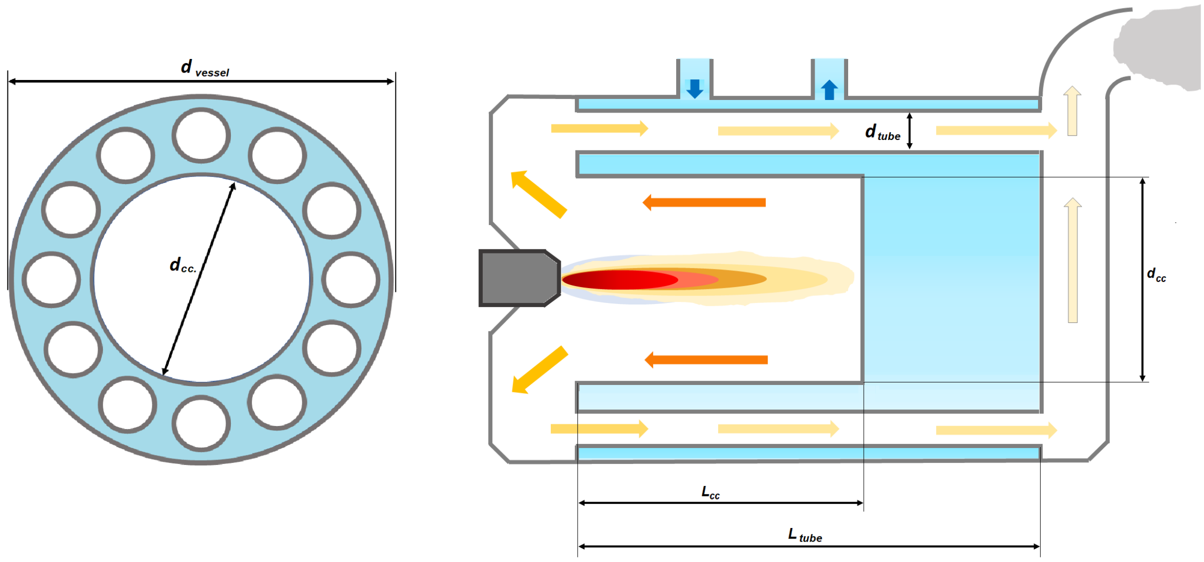

Figure 2: Schematic representation of the flue gas pipes (left) cross section of the experimental set-up (right)

valve, upstream of the fan. Successively, the flame develops on the burner's head and the exhaust flue gases are distributed along the entire combustion chamber, which is sized large enough to manage the considerable flame radiation and heat exchange with respect to the combustion chamber's walls. Once the flue gases reach the bottom of the combustion chamber, their direction is diverted back coaxially, flowing closer to the walls. Subsequently, the flue gases are distributed in the smoke pipes, where the heat is exchanged with the metal walls. At tube's outlet section, flue gases are then discharged into the atmosphere through the chimney.

For each smoke tube three K-type thermocouples [42] have been positioned at the inlet, middle and outlet sections, while, on the water side, five uniformly spaced J-type thermocouples were placed directly on the pipe's skin to measure the surface's temperature gradient along the entire tube axis. The total exhaust fumes mass flow rate is determined employing the stoichiometric calculation [2] starting from the methane volume flow rate ($\dot{V}_{ch4}$) and air excess value (e), measured on the inlet methane pipe and on the boiler's chimney. Successively, the mass flow rate that enters each smoke pipe is derived by the total smoke mass flow rate produced by the burner divided by the total number of the smoke pipes. The pressure drop between inlet and outlet smoke pipe's sections is not measured owing to its low value (as verified by CFD simulations it is lower than 0.5 $mbar$) that can not be read by the pressure probes available at ICI laboratories. The same situation holds for the study conducted by Bisetto et al. [20], in which the pressure drop is not reported. Generally, all registered measurements take into account the instruments' error: the methane flow-meter error band is equivalent to $\pm 0.34\%$ of the reading; the type-K and the type-J thermocouples have an error band of ± 2.5 K and ± 1.5 K respectively; the gas analyzer provide the air excess value with an error band equal to $\pm 0.4\%$ of the acquired value.

Finally, the boiler system has been fully insulated, with the exception of supply and

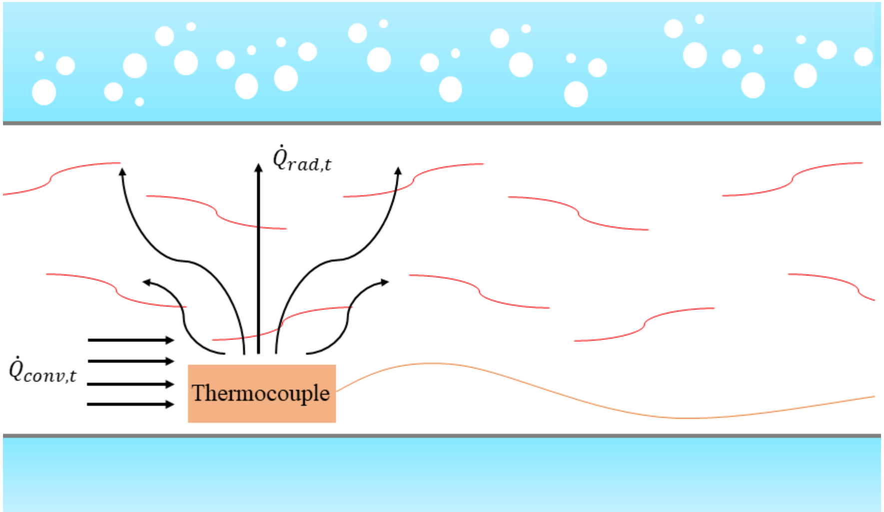

Figure 3: Location of the thermocouple at flue-gas side and representation of considered heat transfer terms

return pipes, to minimize the heat losses from the boiler's shell towards the external environment.

2.2. Uncertainty analysis

The uncertainty analysis section presented has the following two objectives: i) to estimate the flue-gas experimental temperature motivated by the notable radiative heat flux term mechanism which in turns affect the thermocouples readings, ii) then to evaluate the systemic uncertainty on the estimated flue-gas temperature based on the uncertainty of the recorded data. Moreover, these information are used exclusively in the CFD validation procedure, in which the predicted outlet flue-gas temperatures are compared with the corresponding experimental values and their uncertainties (see Sec. 5.2). The measurements for methane flow rate, $\dot{V}_{ch4}$, and air excess value, e, have been manually sampled during the test, and only the declared instrument error has been considered. The uncertainty associated to the measured temperatures is computed as the superposition effect of systemic phenomena due to the presence of the effects of the sampling infrastructure and the ambient in which the sensors are installed. The proposed analysis also investigates the systemic phenomena in which the combined convective and radiative heat transfer mechanisms induce a notable temperature bias of the flue-gas side thermocouples readings, as shown in Fig. 3.

The mentioned systemic phenomenon is described by applying the energy conservation principle at the thermocouple boundaries. The convective heat transfer mechanism occurs along the external surface of the temperature probe and the radiative heat flux is acting between the thermocouple's surface and the surrounding cold walls of the fire-tubes. The steady-state energy balance is expressed as:

$$m_t \; c_{V,t} \, \frac{dT}{dt} = V_t \; \rho \; c_{V,t} \, \frac{dT}{dt} = \dot{Q}_{conv,t} - \dot{Q}_{rad,t} = 0 \; . \tag{1}$$

Therefore, the measured temperature in the given scenario is reduced by the presence of the radiative heat transfer term.

The convective heat transfer is modelled as:

$$\dot{Q}_{conv,t} = h_{conv}\ A_t\ (T_{fg} - T_t), \tag{2}$$

while the convective heat transfer coefficient, h_{conv}, is defined as

$$h_{conv} = \frac{Nu\ \lambda_{fg}}{d_t}. \tag{3}$$

The convective heat transfer mechanism across the cylindrically shaped thermocouple surface is described by the Whitaker equation [43] for turbulent external flows in single spheres, which has the following formulation,

$$Nu = 2 + \left(0.4\ \sqrt{Re} + 0.06\ \sqrt[3]{Re^2}\right)\ Pr^{0.4}\ \left(\frac{\mu_{wall}}{\mu_{fg}}\right)^{0.25}, \tag{4}$$

The flue gas stream across the channel, is defined taking into account the wet cross section between the pipe and the round solid thermocouple, where the wet cross section is calculated using the hydraulic diameter [44], d_{hyd}, defined as

$$d_{hyd} = \frac{2\,(A_{tube} - A_t)}{\pi\,(d_{tube} + d_t)} = (d_{tube} - d_t) \tag{5}$$

while A_{wet} results:

$$A_{wet} = \frac{\pi}{4}\left(d_{tube}^2 - d_t^2\right); \tag{6}$$

The radiative heat flux is modelled applying the gray surfaces model, thus expressing the equivalent radiative thermal resistance as the sum of the combined effects of the thermocouple and surrounding walls with isotropic emissivity values:

$$\dot{Q}_{rad,t} = g_{tot}\ (T_t^4 - T_{wall}^4), \tag{7}$$

where

$$g_{tot} = \sigma\ \frac{A_t}{\dfrac{1-\varepsilon_t}{\varepsilon_t} + \dfrac{1}{F_{t,wall}} + \dfrac{1-\varepsilon_{wall}}{\varepsilon_{wall}}}. \tag{8}$$

The thermocouples installed on the experimental set-up at the flue-gas side are completely surrounded by the neighbouring walls (that physically separate the flue gas from the boiling water). Accordingly, the view factor is assumed to be ideal and equal to $F_{t,wall} = 1$.

Finally, beginning from the energy balance equation under steady-state conditions Eq.1, the temperature difference term, $\Delta T_{rad,conv}$, can be calculated as follows:

$$\Delta T_{rad,conv} = T_{fg} - T_t = \frac{\dot{Q}_{rad,t}}{h_{conv}\ A_t}, \tag{9}$$

therefore, the corrected flue gas bulk temperature T_{fg} is determined using Eq. (9) as

$$T_{fg} = T_t + \Delta T_{rad,conv}. \tag{10}$$

The estimated uncertainty of the Nusselt number is determined as the uncertainty propagation of the measured experimental data and the inherit uncertainty of the Whitaker correlation [45], that are expressed as:

$$u(Nu) = \sqrt{\left(\frac{\partial Nu}{\partial Re}\right)^2 u^2(Re) + u^2_{inh,w}(Nu)}, \tag{11}$$

where

$$\frac{\partial Nu}{\partial Re} = [Pr^{0.4}\left(\frac{\mu_{wall}}{\mu_\infty}\right)^{0.25}](0.4\frac{1}{2\sqrt{Re}} + 0.06\frac{2}{3\sqrt[3]{Re}}), \tag{12}$$

and

$$u_{inh,w}(Nu) = 0.2\ Nu. \tag{13}$$

Where $u(Re)$ is defined as,

$$u(Re) = \frac{d_{hyd}}{A_{wet} \cdot \mu_{fg}} \cdot \dot{m}_{fg}, \tag{14}$$

Following Eq.14, propagated uncertainty over the estimated $u(\dot{m}_{fg})$, the latter is defined provided the relative uncertainty of the flow meter equal to 0.6%. The mass flow rate uncertainty considering a triangular distribution [45] is therefore expressed as,

$$u(\dot{m}_{fg}) = \frac{u(\dot{m}_{fg})_{\%} \cdot \overline{\dot{m}_{fg}}}{2\sqrt{3}}. \tag{15}$$

The propagated uncertainty of the convective heat transfer coefficient is expressed as:

$$u(h_{conv}) = \frac{\lambda_g}{d_t} u(Nu). \tag{16}$$

while finally the temperature difference uncertainty expression is the result of the propagation:

$$u(\Delta T_{rad,conv}) = \left(\frac{\dot{Q}_{rad,t}}{h^2_{conv}\ A_t}\right) u(h_{conv}). \tag{17}$$

In general, the flue gas temperature uncertainty is determined as the combined effect of the two major contributions: the propagated temperature difference dispersion $u(\Delta T_{rad,conv})$ and the repeatability uncertainty of the thermocouple measured quantities. The latter value, which has been sampled across every design point, is equal to the standard deviation of the sampled population. Therefore, the global flue gas temperature is determined as:

$$u(T_{fg}) = \sqrt{u^2(\Delta T_{rad,conv}) + Var(T_t)} \tag{18}$$

Finally, the provided uncertainty estimation of the flue gas temperature is included in the CFD model validation phase.

3. CFD simulations

In the present section, the details of the CFD approach are provided. In particular, the adopted physical models are described and a mesh sensitivity analysis is reported to assess the optimal grid spacing. Finally, the numerical model is validated, comparing the predicted results with experimental data available in literature and measurements performed at ICI Caldaie Lab.

3.1. Numerical set-up

All the simulations of the fire-smoke tubes were performed employing the Ansys Fluent software [46].

The flow-field inside the tubes has been computed using the compressible steady state Reynolds-Averaged-Navier-Stokes (RANS) equations (including gravitational forces) coupled with the two equations $SST\ k-\omega$ turbulence model [47] with Low-Re corrections and enabling the viscous-heating, similarly to the Bisetto et al. [20] and to Eiamsa-Ard [10] works. The energy equation has been activated to consider heat transfer, and the Discrete Ordinates (DO) model [48, 49] has been adopted to simulate radiative heat exchange; despite the small values of the test cases mean beam length, the radiative heat exchange cannot be neglected due to the high inlet temperature. Furthermore, equations for the transport of non-reactive species [50] were considered for all species present in flue gases resulting by the combustion of an air-methane mixture. Derived polynomial functions were used to calculate the dynamic viscosity, the specific heat and the thermal conductivity [51] for each species. The composition-dependent properties for multi-component mixture, *i.e.* the kinematic viscosity, the isobaric and isochoric specific heat and the thermal conductivity were calculated applying the kinetic theory. Finally, the Weighted-Sum-of-Gray-Gases Model (WSGGM) [32] for the estimation of gases emissivity (ε) has been used. A coupled solver has been chosen to solve the resulting system of equations; furthermore, the gradient is discretized using a least-square method, while the second-order upwind discretization scheme is applied to the velocity, energy, turbulence quantities, radiation, and species equations.

At the inlet section the mass flow rate of a single smoke pipe, $\dot{m}_{fg,tube}$, is set, while at the outflow section the static pressure is prescribed. A no-slip boundary condition is set on the tubes internal surface with fixed temperature. Assuming the total flue mass flow rate, $\dot{m}_{tot}$, is uniformly distributed among the smoke-pipes, $\dot{m}_{fg,tube}$ can be computed as

$$\dot{m}_{fg,tube} = \frac{\dot{m}_{tot}}{n_{tubes}}, \tag{19}$$

where n_{tubes} is the number of smoke-pipes, while $\dot{m}_{tot}$ can be computed as

$$\dot{m}_{tot} = \dot{m}_{ch4} + \dot{m}_{air}. \tag{20}$$

The $\dot{m}_{ch4}$ value is obtained by the experimental measurement of the methane volumetric flow rate as

$$\dot{m}_{ch4} = \rho_{ch4}\ \dot{V}_{ch4}, \tag{21}$$

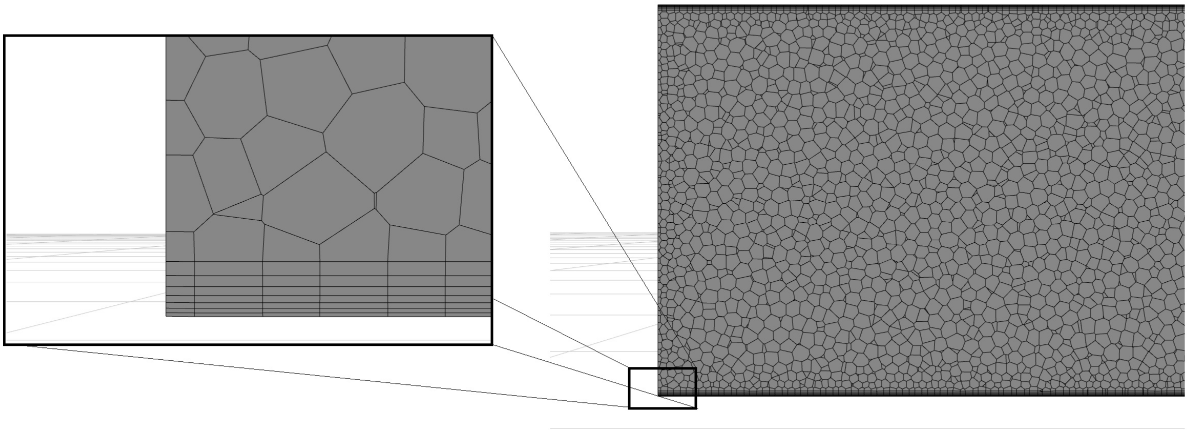

Figure 4: Polyhedrical mesh of the computational domain with a detali of the boundary layer zone

where ρ_{ch4} is the density of methane at atmospheric conditions.

The air mass flow rate, $\dot{m}_{air}$, can be estimated from methane mass flow and the air excess (e), often kept within a range between $0.1 < e < 0.55$ [52] ($e \approx 0.2$ in this work), and strictly dependent on the chemical composition of exhaust flue gases [2], as

$$\dot{m}_{air} = 17.24\ \dot{m}_{ch4}\ (1 + e). \tag{22}$$

The temperature on the internal wall is kept constant along the tube, because the water is evaporating. The temperature value is equal to the mean value of water-temperatures measured on the smoke-tube increased by a temperature difference that accounts for the pipe's steel thermal conductivity, accordingly to the Fourier's law [51].

3.2. Mesh sensitivity analysis

A mesh sensitivity analysis has been performed to identify the grid size that guarantees the grid independence of the results, while minimizing the computational cost. This activity has been performed on a tube characterized by the following dimensions: $D_{tube} = 106.3\ mm$ and $L_{tube} = 3350\ mm$.

At the inlet section, the total mass-flow rate of $\dot{m}_{fg} = 0.01867\ kg/s$, the temperature of $T_{fg,in} = 1000\ K$ and the gas emissivity of $\varepsilon_{fg} = 0.3$ are prescribed. The chemical composition is determined by the air excess value e through the stoichiometric calculation [2] and the following values have been imposed on both inlet and outlet sections: $\%CO_2 = 12.76$, $\%O_2 = 3.66$, $\%H_2O = 10.44$. The static pressure, $p_{out} = p_{atm}$, is imposed on the outflow. A no slip boundary condition is applied to the walls with the imposed temperature of $T_{wall} = 467\ K$, which is assumed to be constant along the entire tube, while the wall emissivity is set to $\varepsilon_{wall} = 0.5$.

Different mesh sizes were considered in a range between $1.72\times$ and 7.97×10^6 polyhedral elements; for all meshes the non dimensional height of the first cell, *i.e.* the y^+, is set around 1 to capture the heat exchange at the wall correctly.

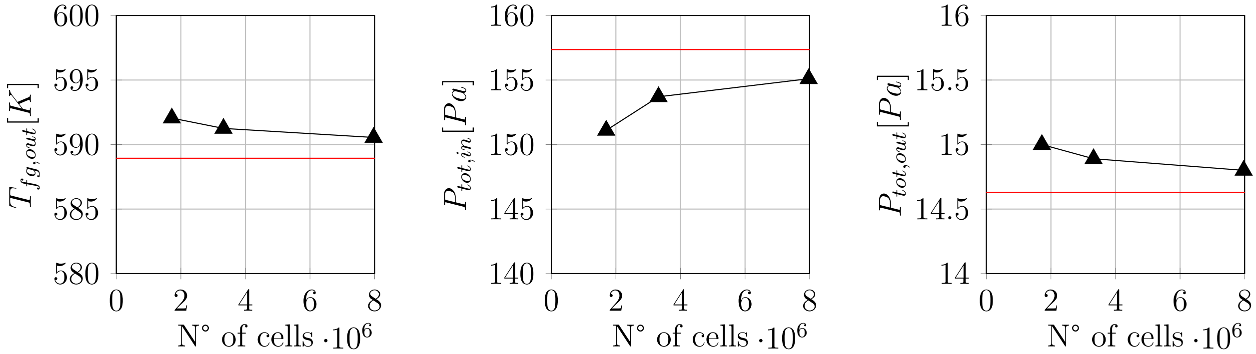

Figure 5: Mesh sensitivity analysis for outlet temperature (left), inlet total pressure (center), and outlet total pressure (right). Red lines represent Richardson's extrapolated values

The values used to compare the different meshes are the mass-weighted-average temperatures ($T_{fg,out}$) and the area-weighted-average total pressure on the inlet ($P_{tot,in}$) and outlet ($P_{tot,out}$) surfaces. The reference values ($T_{fg,out-Rich.}$, $P_{fg,in-Rich.}$ and $P_{fg,out-Rich.}$) have been calculated utilizing the Richardson theory [53] and are shown in Fig. 5 as red lines. Table 2 summarizes the predicted results. The medium mesh (see Fig.4) has been selected for the following simulations as it guarantees a deviation below 2.5% for the quantities of interest and it reduces the computational cost with respect to the finer mesh.

	N. of elements	$T_{fg,out}[K]$	$\Delta\%$	$P_{tot,in}[Pa]$	$\Delta\%$	$P_{tot,out}[Pa]$	$\Delta\%$
Coarse	1 720 000	592.02	-0.52 %	151.51	3.71 %	15.00	-2.53 %
Medium	3 320 000	591.65	-0.46 %	153.72	2.31 %	14.89	-1.77 %
Fine	7 970 000	590.55	-0.27 %	155.18	1.38 %	14.80	-1.16 %
Richardson	/	588.94	/	157.36	/	14.63	/

Table 2: Mesh sensitivity analysis. Predicted outlet temperature, $T_{fg,out}$, inlet total pressure, $P_{tot,in}$, and outlet total pressure, $P_{tot,out}$, and the corresponding error with respect to the Richardson extrapolated values for different mesh density (coarse, medium and fine)

4. Reduced FVM modelling description

In the present section, following the development of a CFD numerical approach, a less computationally intensive, yet detailed, physical based model is implemented and the corresponding correlations are discussed. The key objective of the reduced Finite Volume Method (FVM) modelling is simulating the behaviour (heat transfer and pressure drop along the tube axis) of flue gases in fire-tube boilers fed by natural gas. The flue gas flow is considered to be injected at tubes' inlet section, while ideal mixing and complete flow development is assumed along the whole tubes' length. The convective and radiative heat transfer mechanisms are assumed only along the radial direction, while the local conditions are determined thanks to a simplified FVM approach. The Finite Volume Method is implemented utilizing discrete cylindrical shaped volumes, in which homogeneous conditions are considered. The frontal surface of the discrete volume element devides them along the tube axis, while the lateral surface defines the boundary separating the flue gas volume element from the stationary wall. The simulated parameters are the pressure and the temperature defined for each discrete volume element. For determining the the flue gas mixture's properties, real gas behaviour is assumed; hence, a methodology based on Helmotz's energy formulation is applied [54].

4.1. Energy balance and heat transfer equations

The FVM architecture, represented in Fig. 6, describes the energy flow terms, where the heat balance equation of each i-th volume element is expressed as:

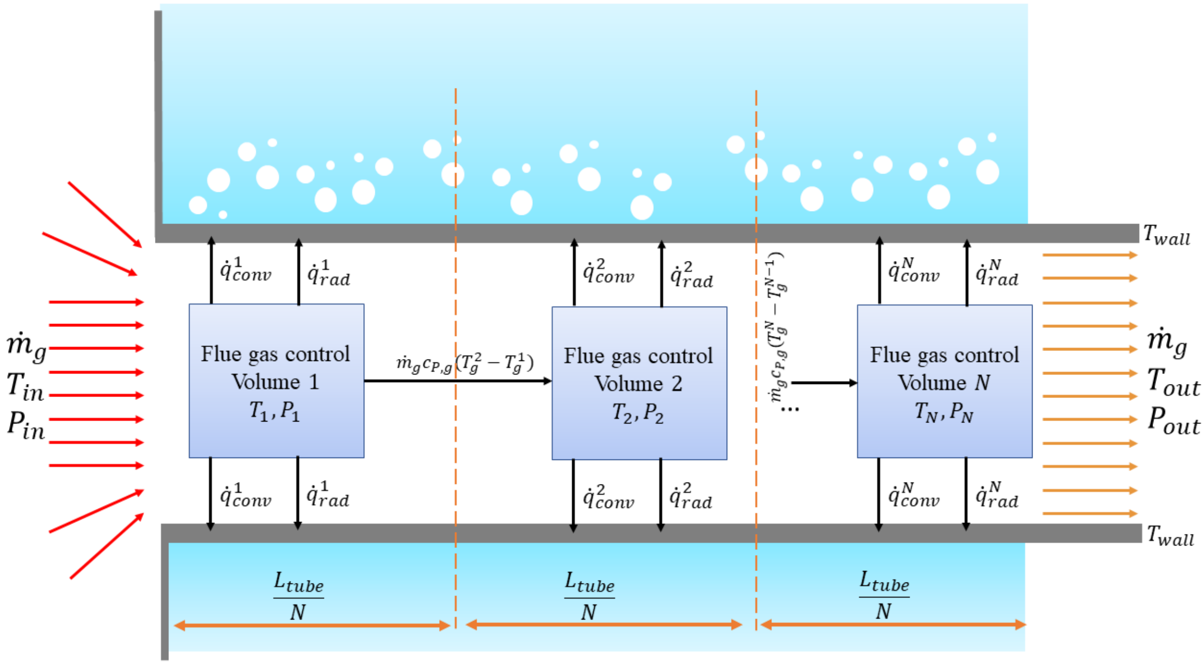

Figure 6: Developed Finite Volume Method (FVM) architecture for a cylindrical horizontal fire-tube

$$\frac{d}{dt}\left[(\rho_{fg}\ V)\ \ c_{V,fg}\ T^i_{fg}\right] = \dot{m}_{fg}\ \bar{c}_{P,fg}\ (T^{i-1}_{fg} - T^i_{fg}) - \dot{Q}^i_{rad} - \dot{Q}^i_{conv}, \tag{23}$$

where, as a steady-state regime is considered, the following equation holds:

$$\frac{d}{dt}\left[(\rho_{fg}\ V)\ \ c_{V,fg}\ T^i_{fg}\right] = 0. \tag{24}$$

The convective heat transfer equation is expressed as:

$$\dot{Q}^i_{conv} = h^i_{fg}\ \frac{2\pi R_{tube} L_{tube}}{N}\ (T^i_{fg} - T_{wall}), \tag{25}$$

where h^i_{fg} is based on the empirical Dittus-Boelter [25] correlation (valid for turbulent flow of smooth tubes under gas cooling process), and can be defined as

$$h^i_{fg} = \frac{0.023 k^i_{fg}}{2R_{tube}}\ Re_i^{0.8}\ Pr_i^{0.3}, \tag{26}$$

where the bulk flow properties are evaluated. Equation (26) is valid for a moderate radial temperature gradient ($|T^i_{fg} - T_{wall}|$), while for higher gradient values more complex correlations are adopted: Sieder and Tate [55] equation and the Gnielinski [26, 27] correlation. The Sieder and Tate equation evaluates the properties at bulk flow condition with the exception of the the dynamic viscosity, which is evaluated at the wall, and is defined as:

$$h^i_{fg} = \frac{0.027 k^i_{fg}}{2R_{tube}}\ Re_i^{0.8}\ Pr_i^{1/3} \left(\frac{\mu^i_{fg}}{\mu_{wall}}\right)^{0.14}. \tag{27}$$

The Gnielinski [26, 27] correlation, deviates from the previous formulations, as it employs the friction factor estimated using the Filonienko's [56] correlation:

$$h^i_{fg} = \frac{k^i_g}{2R_{tube}} \frac{f/8\ (Re^i - 1000)\ Pr_i}{1 + 12.7\ \sqrt{f/8}\ (Pr_i^{2/3} - 1)} \left[1 + \left(\frac{d_w}{L}\right)^{2/3}\right] \left(\frac{Pr^i_{fg}}{Pr_{wall}}\right)^{0.11}. \tag{28}$$

The radiative heat transfer term is expressed as

$$\dot{Q}^i_{rad} = g^i_{fg} \frac{2\pi\ R_{tube}\ L_{tube}}{N}\ (T^4_{fg,i} - T^4_{wall}), \tag{29}$$

where g^i_{fg} is the equivalent radiative thermal resistance defined by:

$$g^i_{fg} = \sigma\ \frac{1}{\frac{1-\varepsilon_w}{\varepsilon_w} + \frac{1}{\varepsilon^i_{fg}}}. \tag{30}$$

Following the approach proposed by Smith et al. [32], the gases' local emissivity is estimated as the sum of the polynomial coefficients with respect to the CO_2 and water vapour partial pressure multiplied by the average path length:

$$\varepsilon^i_{fg} = \sum_{j=1}^{J}\ a_{\varepsilon,j}\ (T_i)\ [1 - e^{k_j PS}], \tag{31}$$

where the weighting factor $a_{\varepsilon,j}(T^i)$ represents the fractional amount of black body spectral energy of the k_j-th gas species. The temperature dependency of the mentioned weighting factors is expressed by a polynomial formulation as:

$$a_{\varepsilon,j}\ (T_i) = \sum_{h=1}^{H} b_{\varepsilon,j,h}\ T^{h-1}. \tag{32}$$

In case of natural gas combustion, the partial pressure ratio between the vapour content and CO_2 molar concentration in the flue gases is close to 2. Thus, the polynomial gas temperature coefficients considered for $\frac{P_{H_2O}}{P_{CO_2}} \approx 2$ are reported in Table 3.

The proposed model is valid for a gas temperature in the range 600 $K < T_g <$ 2400 K and a total pressure equal to 1 atm.

j	k_j	$b_{\varepsilon,j,1} \cdot 10^1$	$b_{\varepsilon,j,2} \cdot 10^4$	$b_{\varepsilon,j,3} \cdot 10^7$	$b_{\varepsilon,j,4} \cdot 10^{11}$
1	0.4201	6.508	-5.551	3.029	-5.353
2	6.516	-0.2504	6.112	-3.882	6.528
3	131.9	2.718	-3.118	1.221	-1.612

Table 3: Smith's grey-gases emissivity temperature polynomial coefficients for $\frac{P_{H_2O}}{P_{CO_2}} \approx 2$

4.2. Head losses models

The viscosity of the flue gasses near the wall generates friction losses and, as a consequence, a pressure drop along the tube's longitudinal axis. The tubes' distributed head losses can be described analytically as

$$\Delta P_i = f_{d,i} \, \frac{8 \; L_i \; \dot{m}_{fg}^2}{\pi^2 \; D_{tube}^5 \; \rho_{fg}}, \tag{33}$$

where $f_{d,i}$ is the Darcy friction factor [57] evaluated at the i-th element.

Explicit friction factor correlations are thus employed and their effect on the precited results is investigated in Sec. 5.4. The Petukhov equation [58], which is valid for fully developed turbulent flows ($Re_D > 10^4$), is expressed as:

$$f_d = (1.82 \; ln(Re) - 1.64)^{-2}. \tag{34}$$

A wider range of operating conditions is allowed by the Filonenko correlation [56], which is valid in the turbulent regime region within the range $3 \cdot 10^4 < Re_D < 10^7$. This correlation is based on the previous Petukhov equation for smooth tubes and is defined as:

$$f_d = (0.790 \; ln(Re) - 1.64)^{-2}. \tag{35}$$

Recently, more accurate friction factors correlations have been developed. The Fang et al. [37] expression developed for smooth pipes is written as:

$$f_d = 0.25 \left[log \left(\frac{150.39}{Re^{0.98865}} - \frac{152.66}{Re} \right) \right]^{-2}, \tag{36}$$

and it is valid in the range $3 \cdot 10^3 < Re_D < 10^8$ with a proposed mean absolute relative error (MARE) of 0.022%.

The results of the physical based correlations are compared with the output of the CFD simulations for the same operating conditions. The scoring functions are the corresponding absolute and relative error computed for the estimated temperature and pressure of the flue gases at prescribed cross sections. The mean absolute relative error (MARE) is a percentage based index defined as:

$$MARE(f) = \frac{1}{N_{val}} \sum_{i=1}^{N_{val}} \frac{|f(i)_{estimated} - f(i)_{validation}|}{f(i)_{validation}} \cdot 100 \tag{37}$$

4.3. Sensitivity analysis on the size of the volume element

An investigation on the effect of finite volume's size, aiming at achieving solution independence, is performed. Flue-gas side's finite volume element resolution is defined as:

$$res_{el} = \frac{L_{tube}}{N}, \tag{38}$$

where res_{el} represents the thickness of an element of the cylindrical volume discretization and is considered constant along the tubes' main axis. It varies in the range $5 \cdot 10^{-4}$ $m/element$ and 1 $m/element$. The temperature and pressure mean absolute errors, computed employing the selected heat transfer models and friction factor equations, have been chosen to analyze the influence of the element resolution, as shown in Fig. 7.

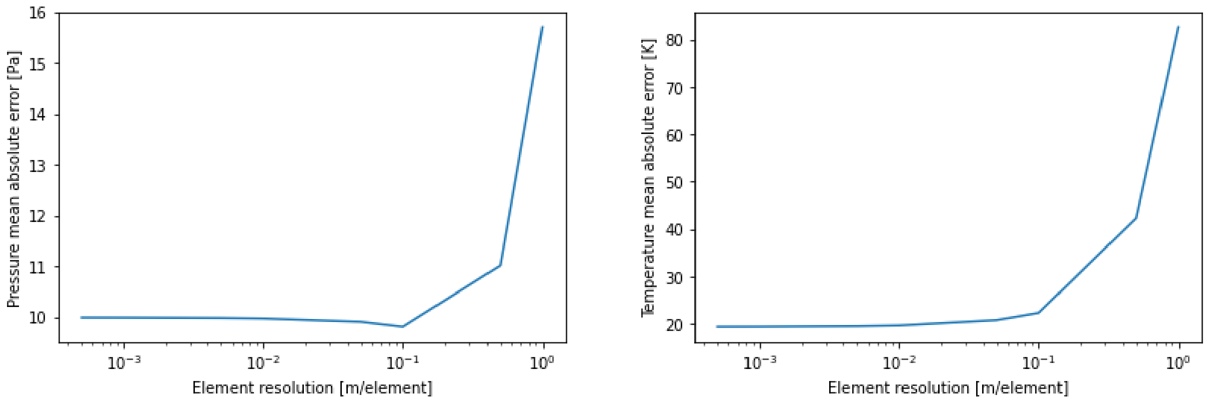

Figure 7: Logarithmic scale determined temperature and pressure mean absolute error trends with various finite volume geometrical size resolutions

The results demonstrates the independence between the model's error and the volume size (of the finite volume fire-tube discretization method) at 10^{-2} $m/element$ for the pressure estimation. However, temperature estimation reaches the mesh independence at 10^{-3} $m/element$. The lower value has been selected as it maximizes the accuracy, while the computational cost is still relatively low, as only 1D simulations are considered.

4.4. Physical models optimization procedure

In the present section, the optimization procedure, implemented to determine the optimal coefficients of the convective heat transfer model and the distributed pressure losses correlation, is described. This procedure aims at reducing the estimation bias, performing a tuning procedure on the coefficients of selected convective heat transfer and the Fanning friction factor models over the wide range of operating conditions of the validation data-set. Initially, the accuracy of all implemented Nusselt and friction factor correlations (available in the literature) is assessed, comparing the estimations with the CFD results. The coefficients of the correlations that minimize the estimation errors are optimized. It is noteworthy that, while tuning the coefficients of the selected convective heat transfer correlation, the methodology indirectly addresses the global heat transfer phenomena composed of convection and thermal radiation components.

The optimization framework is based on a genetic algorithm [59–61]. In particular, a Non-Dominant Sorting Genetic Algorithm is implemented (NSGA-II) [62] for its fast convergence rate to an optimal Pareto front. Taking into account the simultaneous influence of temperature and pressure in the computation of flue-gas real gas mixture properties [54], two separate objective functions are defined to separately minimize the temperature and differential pressure's mean absolute error (MAE). The optimization problem can be described as

$$\min f_1 = min\left(\frac{1}{N_{validation}}\sum_{i=1}^{N_{val}}|T_{estimated,i} - T_{validation,i}|\right), \tag{39}$$

$$\min f_2 = min\left(\frac{1}{N_{validation}}\sum_{i=1}^{N_{val}}|P_{estimated,i} - P_{validation,i}|\right). \tag{40}$$

Moreover, each coefficient (to be tuned) is subjected to a lower and upper bound. Finally, once the Pareto front is obtained, the point $(f_{1,i}, f_{2,i})$ of the Pareto that minimizes the euclidean distance, d, from the origin is chosen as the optimal solution, *i.e.*

$$\min |d(f_{1,i}, f_{2,i})| = \min\sqrt{f_{1,i}^2 + f_{2,i}^2}, \tag{41}$$

where i is the i-th point of the Pareto front.

5. Results and discussions

5.1. Results of the experimental activity

Different experimental tests were carried out, varying the thermal power and air excess value to modify the chemical composition of the flue gases. Accordingly, five different operating conditions have been tested, modifying methane's volumetric-flow rate and the air excess value. The measurements have been corrected to consider the radiant heat dissipation of the thermocouples, as reported in Sec. 2.2.

Table 4 summarizes the measurements. The values reported for each design point refer to the corresponding average sampled values that are obtained in the corresponding test interval. The collected experimental temperatures include also the systematic uncertainty $u(T)$ (see Sec.2.2).

5.2. Validation of the CFD set-up

The CFD simulations have been validated with both experimental data available in literature [20] and data provided by ICI laboratory.

Experimental measurements available in [20] have been obtained on a hot water boiler (fed by methane and air) with a nominal power of 90 kW. In particular, the inlet and outlet temperatures and pressures of a third gas-pass tube with a diameter of 36.4 mm and a length of 826 mm were measured, using K-thermocouples on the flue gas side and on the inlet section. The CFD boundary conditions, i.e. the mass flow rate, $\dot{m}_{fg}$, the inlet temperature, $T_{fg,in}$, the wall temperature, $T_{wall,int}$, and the outlet pressure, P_{out}, and the

Design Points	1	2	3	4	5
$\dot{V}_{ch4}$ $[Nm^3/h]$	3.99	4.12	3.53	4.99	4.51
e	0.29	0.29	0.5	0.31	0.55
$T_{fg,in}$ $[K]$	808	899	829	934	892
$u(T_{fg,in})$ $[K]$	24.63	27.49	20.59	27.96	23.19
$T_{fg,out}$ $[K]$	615	627	600	685	666
$u(T_{fg,out})$ $[K]$	14.83	14.65	12.51	17.09	14.37
T_{wall} $[K]$	348.4	348.7	353	354.4	355
$u(T_{wall})$ $[K]$	0.17	0.27	0.59	0.49	0.26

Table 4: Experimental measured quantities on Hot-Water-Boiler (HWB)

simulation results, i.e. the outlet temperature, $T_{fg,out-CFD}$, are reported in Tab. 5. A good agreement for all considered operating conditions in terms of predicted outflow temperature, $T_{fg,out}$, is demonstrated by the deviation, $\Delta T_{fg,out}$, with respect to the experimental data, which is always below 4%.

Design Points	1	2	3	4
$\dot{m}_{fg} \cdot 10^4$ $[kg/s]$	14.37	15.80	16.62	17.86
e	0.216	0.199	0.193	0.20
$T_{fg,in}$ $[K]$	808	827	834	844
P_{out} $[Pa]$	0	0	0	0
$T_{wall,int}$ $[K]$	350.7	349.9	350.3	350.8
$T_{fg,out-ref}$ $[K]$	582	606	616	626
$T_{fg,out-CFD}$ $[K]$	581	593	597	602
$\Delta T_{fg,out}$ %	0.10%	2.15%	3.08%	3.83%
$\overline{Re}$	1627	1747	1821	1938

Table 5: CFD validation setup with respect to data provided by Bisetto et al. [20]. $\dot{m}_{fg}$ is the massflow rate, $T_{fg,in}$ the inlet temperature, $T_{wall,int}$ the wall temperature, P_{out} the outlet pressure, $T_{fg,out-CFD}$ the predicted outlet temperature, $T_{fg,out-ref}$ the outlet reference temperature, $\Delta T_{fg,out}$ the deviation, and $\overline{Re}$ the mean Reynolds number for the pipe

A second set of experimental measurements has been used to validate the CFD set-up. In particular, the data has been provided by the ICI laboratory through an experimental campaign on a 60 kW two-pass fire Hot-Water-Boiler (HWB). A single pipe with a diameter $d = 41.3$ mm and a length $L = 620$ mm has been considered for the CFD simulations. Mass flow rate, temperature, and chemical composition have been prescribed at the inlet surface, no slip boundary condition with fixed temperature has been set at the tube wall, while at the outflow section the static pressure is set to 0 Pa.

Table 6 summarizes the CFD boundary conditions, the experimental outflow temperatures, the numerical predicted outlet temperatures with both laminar and turbulent models, the non-dimensional numbers that characterize the fluid flow behaviour and the total and ra-

Design Points	1	2	3	4	5
$\dot{m}_{fg} \cdot 10^4\ [kg/s]$	15.26	15.76	15.61	19.37	20.58
e	0.29	0.29	0.50	0.31	0.55
$T_{fg,in}\ [K]$	808	899	829	934	892
$P_{stat,out}\ [Pa]$	0	0	0	0	0
$T_{wall,int}\ [K]$	350.4	350.7	355.0	356.4	357.0
$T_{fg,out-exp}\ [K]$	615	627	600	685	666
$T_{fg,out-CFD}\ (Laminar)\ [K]$	609	656	625	705	692
$\Delta T_{fg,out}\ \%$	0.9 %	-4.7 %	-4.1 %	-2.9 %	-3.9 %
$T_{fg,out-CFD}\ (SST\ k-\omega)\ [K]$	611	637	609	693	674
$\Delta T_{fg,out}\ \%$	0.7 %	-1.6 %	-1.5 %	-1.1 %	-1.2 %
$\overline{Gr} \cdot 10^3$	48.54	50.47	56.67	35.26	37.67
$\overline{Re} \cdot 10^3$	1.49	1.47	1.7	1.92	1.89
$\overline{Ri} \cdot 10^{-2}$	2.2	2.4	2.4	1.2	1.1
$\dot{Q}_{tot}\ [W]$	-398	-517	-419	-644	-598
$\dot{Q}_{rad}\ [W]$	-83	-115	-84	-136	-111
$\Delta\dot{Q}_{rad}\ [\%]$	20.8 %	22.3 %	20.1 %	21.1 %	18.6 %

Table 6: CFD validation setup with respect to experimental measurements on a HWB provided by ICI laboratory. $\dot{m}_{fg}$ is the massflow rate, $T_{fg,in}$ the inlet temperature, $T_{wall,int}$ the wall temperature, P_{out} the outlet pressure, $T_{fg,out-CFD}$ the predicted outlet temperature, $T_{fg,out-exp}$ the outlet experimental temperature, $\Delta T_{fg,out}$ the deviation, and $\overline{Re}$ the mean Reynolds number for the pipe, $\overline{Gr}$ the mean Grashof number for the pipe, $\overline{Ri}$ the mean Richardson number for the pipe, $\dot{Q}_{tot}$ the exchanged total heat, $\dot{Q}_{rad}$ the exchanged radiative heat, $\Delta\dot{Q}_{rad}$ the percentage of the radiative heat exchanged over the total heat exchanged

diant heat exchange through the pipe wall. While in the previous validation, the same CFD set-up proposed by Bisetto et a. has been adopted, characterized by the use of the $SST\ k-\omega$ turbulence model, despite the low Reynolds numbers, in this test case the predicted results provided by laminar and turbulence ($SST\ k-\omega$) models have been compared. The temperature and density flow fields depicted in Figs. 8 and 9 show a substantial agreement. To extend the CFD setup validity to higher Reynolds numbers, the $SST\ k-\omega$ turbulence model with Low-Re corrections and viscous-heating has been chosen for the generation of the data-set required by the optimization process. Moreover, the high temperature gradient generates large differences in the density field, and the buoyancy forces become no more negligible with respect to the inertial contribution, thus bringing the flow into a condition close to mixed convection. This behaviour is also confirmed by the calculation of Richardson Number [51], defined as:

$$Ri = \frac{Gr}{Re^2} = \frac{\Delta\rho\ \vec{g}\ D^5\ \overline{\rho}\ \pi^2}{16\ \dot{m}^2_{fg,tube}}. \tag{42}$$

The Ri number indicates if the convection heat transfer is forced ($Ri << 1$), natural ($Ri >> 1$) or mixed ($Ri \approx 1$). The Ri values obtained during the validation analysis on HWB

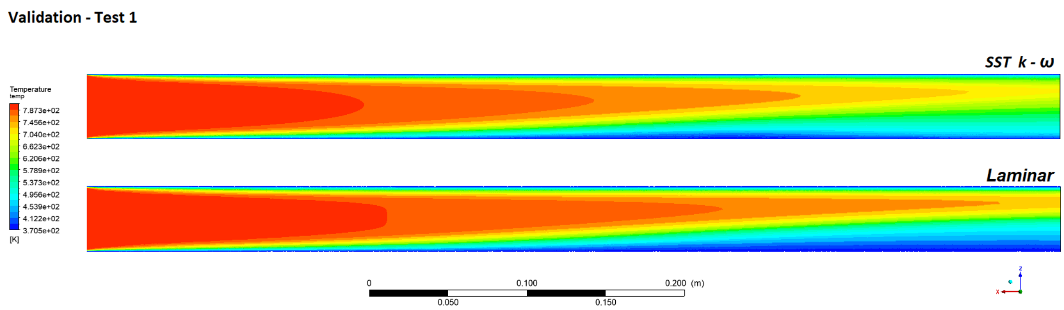

Figure 8: Temperature contours obtained with Laminar and $SST\ k-\omega$ turbulence models for the design point 3

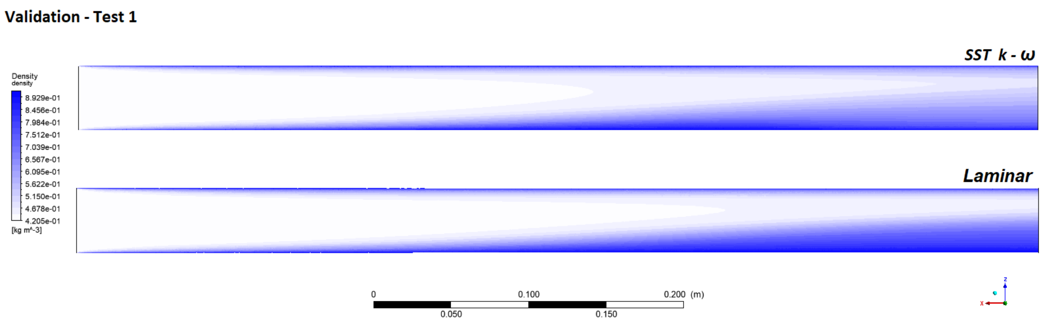

Figure 9: Density contours obtained with Laminar and $SST\ k-\omega$ turbulence models for the design point 3

(see Tab.6) indicate that, although the forced convection is predominant, the gravitational effects cannot be avoided, especially for design points 1, 2 and 3. The outlet temperature deviation between the numerical results obtained with $SST\ k-\omega$ turbulence model and the experimental data, is always below 1.5% and within the estimated uncertainty (see Tab. 4).

Table 6 reports also the total heat exchanged and the radiative component, which is approximately 20% of the total heat exchanged through the pipes' wall. Despite the small values of mean beam length, the radiative heat exchanged cannot be neglected for the high inlet temperature. The good agreement between numerical and experimental results confirmed also the validity of the DO model [48, 49] to predict the radiative heat exchange.

5.3. *Results of the CFD simulations*

Exploiting the numerical set-up validated in Sec. 5.2, the simulations of the flue gas inside generic smooth horizontal smoke pipes, representative of the second and third passage, are performed for different design parameters, *i.e.* the tube internal diameter, the gas mass flow rate, the gas inlet temperature and the internal wall temperature.

The considered variables are both geometrical and thermo-physical to assess their influence on the heat exchange phenomena and on the distributed pressure losses between the flue gas flow and the pipe's wall. Figure 10 shows logic scheme followed to define the design points variables, considering a fixed pipe length of 2500 mm. Boundary conditions were prescribed to consider different boiler operating conditions, ranging from the lower to the higher

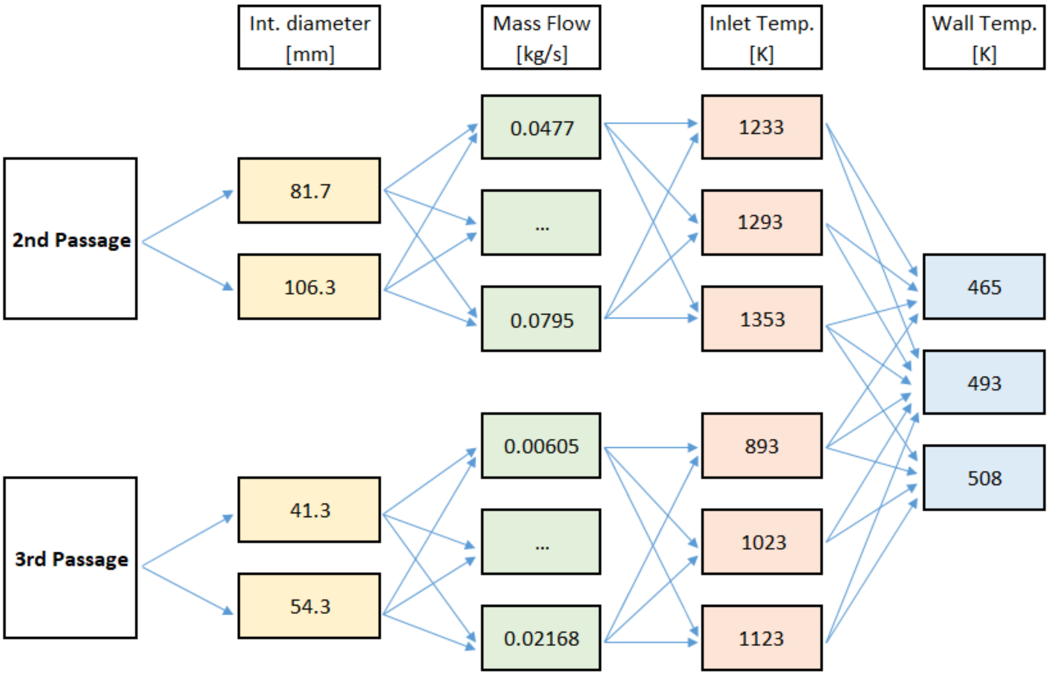

Figure 10: Data-set logic scheme performed with CFD simulations

maximum thermal power typically exchanged on medium-size steam boilers' pipes. Globally, 72 and 87 simulations were performed for the second and third passage, respectively. The CFD simulations performed have Reynolds numbers in the range $3000 < Re < 28000$.

5.4. Results of physical equations' comparison

In this section, a description of the estimation bias of the implemented physical correlations is provided. The present validation task is performed by comparing the empirical models with the validation CFD dataset (see Sec. 5.3), which considers a wide range of geometrical and operating conditions. The evaluations are conducted separately applying a constant volume element resolution, identified by the sensitivity analysis (see Sec. 4.3). Each evaluation estimates the temperature and pressure trend along the tube's axis for every element in the validation data-set and for all implemented physical correlation. Statistical indicators are here employed and their results are reported in Table 7. The analysis are carried out separately for the internal heat transfer models and the head losses correlations.

Results clearly indicate the greater accuracy of the Gnielinski model over the wide set of validation data. In addition, the Gnielinski convective heat transfer equation is more suitable for the current operating conditions, characterized by considerable radial temperature gradients.

The validation of the differential pressure losses models shows the greater accuracy of the Fang correlation [37], with respect to the Petukhov and Filonienko models.

It is also worth noticing that, although several physical based convective heat transfer equations are analyzed, the proposed heat transfer model applies the gray gas radiative model

Model	MAE	$MARE[\%]$	Var	$St.Dev$
Dittus-Boelter [25]	84.12 $[K]$	9.59	1714.89 $[K^2]$	41.41 $[K]$
Sieder-Tate [55]	19.73 $[K]$	2.25	214.07 $[K^2]$	14.63 $[K]$
Gnielinski [27]	17.07 $[K]$	1.95	86.53 $[K^2]$	9.30 $[K]$
Petukhov [58]	20.45 $[Pa]$	-	399.08 $[Pa^2]$	19.98 $[Pa]$
Filonenko [56]	26.45 $[Pa]$	-	530.08 $[Pa^2]$	23.02 $[Pa]$
Fang [37]	9.30 $[Pa]$	-	612.67 $[Pa^2]$	24.75 $[Pa]$

Table 7: Validation of the heat transfer and pressure drop models with respect to the CFD data-set

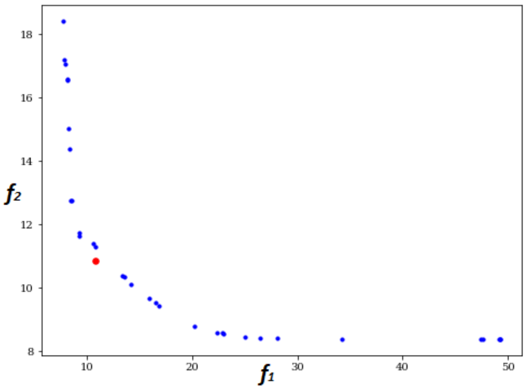

(a) The Pareto front of the performed multi-objective optimization. The selected optimal point is depicted in red

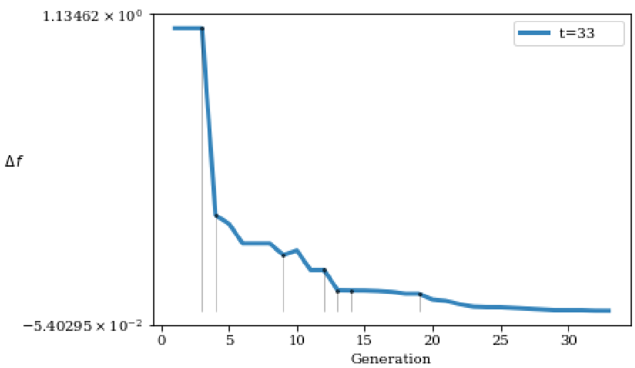

(b) Running metric [63] results over the set of generations

Figure 11: Pareto front and running metric

using the Smith weighted sum of gray gas emissivity (WSGGM) polynomial coefficients (see Eq. (31)).

5.5. Physical models' optimization

In the present section an optimization procedure is described, which aims to reduce the estimation bias of the Gnielinski convective heat transfer equation, and the Fang friction factor. A tuning phase over CFD data-set is performed, and 11 variables are optimized subject to a defined research space contiguous with the former coefficients of the equations. The choice of employed objective functions is motivated by the comparable scale, while estimating both temperature and pressure MAE. The final (last generation's) Pareto front, which is obtained by the used genetic based optimization algorithm, is shown in Fig.11, such as the optimization algorithm's convergence diagram applying the running metric [63] procedure between each generation.

The proposed index measures the generational variation within the objective space. The results indicate that the algorithm reaches an acceptable convergence conditions after 33 generations. Once the last Pareto set of solutions is obtained, the solution with the minimum euclidean distance from the origin is chosen as the optimal. Table 8 compares the accuracy of the models with optimized and standard coefficients.

$$Nu^i_{fg} = \frac{f_{fg,d}/7.5630 \cdot (Re^i - 987.4441)Pr_i}{1.0404 + 12.0090\sqrt{f/7.5630} \cdot (Pr_i^{0.6687} - 1)} \left[1 + \left(\frac{d_w}{L}\right)^{0.6012}\right] \left(\frac{Pr^i_{fg}}{Pr_{wall}}\right)^{0.13} \tag{43}$$

$$f^i_{fg,d} = 0.2054 \left[log\left(\frac{146.9152}{Re_{D,i}^{0.976}} - \frac{153.7099}{Re_{D,i}}\right)\right]^{-2} \tag{44}$$

Model	MAE	$MARE[\%]$	Var	$St.Dev$
Convective heat transfer				
Gnielinski [27]	17.07 $[K]$	1.95	86.53 $[K^2]$	9.30 $[K]$
Convective heat transfer optimized correlation	10.75 $[K]$	1.24	50.09 $[K^2]$	7.08 $[K]$
Friction factor models				
Fang [37]	9.30 $[Pa]$	-	612.67 $[Pa^2]$	24.75 $[Pa]$
Friction factor optimized correlation	10.85 $[Pa]$	-	634.44 $[Pa^2]$	25.19 $[Pa]$

Table 8: The comparison between the performance of the Optimized correlations (for heat transfer and pressure drop estimation) with the respect to the baseline equations available in the literature

The results demonstrate an improvement of the accuracy for the convective heat transfer correlation, while the performance of the optimized model for the distributed pressure drop is slightly worse than the baseline model proposed by Fang [37]. This behaviour can be ascribed to the joint influence of pressure and temperature values, while estimating the flue-gas properties through the mentioned real-gas model.

It is finally worth mentioning that although a set of novel correlations has been identified, their application is subject to the considered operating conditions.

6. Conclusions and future works

The present study aimed at analyzing the heat transfer performances and head losses models of flue-gases in smooth horizontal Fire-tubes on a wide range of operating conditions.

Initially, experimental measurements were performed in fire-tubes to describe the physical behaviour of flue gases while exchanging heat with a surrounding liquid media under steady-state regime. A thorough experimental uncertainty analysis was implemented and uncertainties of the propagated variables were consequently estimated.

Subsequently, an accurate CFD model was used to predict the flow field in smoke pipes under different operating conditions, in order to create a large data base that will be used as validation data-set. The physical models adopted in the CFD set-up were validated comparing the predicted results with experimental data available in literature and with the measurements performed in the initial phase. A good agreement between the results of the CFD simulations and the measured in-tube heat transfer and distributed pressure drops physical phenomena was observed.

In the second part, a simplified 1-D FVM based model was developed, assessing the convective and radiative heat transfer together with distributed friction factor equations of the fire-tube's flue gas side. An initial assessment of finite volume resolution resulted in an optimal 1 $mm/element$ length of the volume discrete element as the trade-off between acuuracy and computational cost. A wider set of operating conditions was simulated employing the CFD approach, thus assessing the temperature and absolute pressure trends along the tube longitudinal axis, which consequently expanded the available set of scenarios. Furthermore, the performance of a set of traditional convective heat transfer equations and friction factor models was assessed through determining the models' resulting bias with respect to the available set of validation data. Additionally, the Smith grey-gas emissivity model was implemented, which is based on a weighted sum of gray gas coefficients and addresses the radiative emissivity of hot gray gases present in methane exhaust flue-gas species.

Successively, it was demonstrated that the Gnielinski equation leads to the lowest estimation error (with respect to the validation dataset), which also indicates the notable effect caused by the temperature difference between the bulk flow and the metal wall side. Finally, a multi-objective optimization (MOGA) procedure was designed aiming at reducing the models' error. A number of 11 coefficients of the Gnielinski and Fang equations were selected as optimization variables. Coefficients were tuned subject to the minimization of the deviation between the estimated values of flue gas temperature and pressure with respect to the validation dataset, which was determined at 12 validation cross-sections along the fire-tube longitudinal axis. The optimal correlations show an improved convective heat transfer estimation capability in a wide set of simulated operating conditions, while drastically reducing the computational cost (compared to the more computationally expensive CFD models). The proposed methodology can be applied to similar cases providing improvements over simplified approaches that are commonly employed in the literature.

It is also noteworthy that the achieved reduction in the temperature estimation errors using the proposed approach based on optimized correlations, allows decreasing the estimation uncertainties during the preliminary design of Fire-tube boilers.

7. Acknowledgments

The authors would like to thank ICI Caldaie S.p.A. in providing technical and experimental support for this research project. The corresponding activities, managed by ICI Caldaie, have been conducted in the context of the Ecovapor project. Additionally, we gratefully acknowledge the support of NVIDIA Corporation with the donation of computer hardware used for this research.

References

[1] M. Barma, R. Saidur, S. Rahman, A. Allouhi, B. Akash, S. M. Sait, A review on boilers energy use, energy savings, and emissions reductions, Renewable and Sustainable Energy Reviews 79 (2017) 970–983.

[2] D. Annaratone, Steam Generators: Description and Design, 2008. doi:10.1007/978-3-540-77715-1.

[3] A. Kumar, M. Kumar, S. Chamoli, Comparative study for thermal-hydraulic performance of circular tube with inserts, Alexandria Engineering Journal 55 (01 2016). doi:10.1016/j.aej.2015.12.013.

[4] A. Verma, M. Kumar, A. Patil, Enhanced heat transfer and frictional losses in heat exchanger tube with modified helical coiled inserts, Heat and Mass Transfer 54 (10 2018). doi:10.1007/s00231-018-2347-x.

[5] B. Cetin, K. Güler, M. Aksel, Computational Modeling of Vehicle Radiators Using Porous Medium Approach, 2017. doi:10.5772/66281.

[6] M. Hatami, M. Jafaryar, D. Ganji, M. Gorji-Bandpy, Optimization of finned-tube heat exchangers for diesel exhaust waste heat recovery using cfd and ccd techniques, International Communications in Heat and Mass Transfer 57 (2014) 254 – 263. doi:https://doi.org/10.1016/j.icheatmasstransfer.2014.08.015.

[7] M. Sheikholeslami, M. Jafaryar, A. Shafee, Z. Li, R. Haq, Heat transfer of nanoparticles employing innovative turbulator considering entropy generation, International Journal of Heat and Mass Transfer 136 (03 2019). doi:10.1016/j.ijheatmasstransfer.2019.03.091.

[8] L. Erbay, N. Uğurlubilek, Ö. Altun, B. Dogan, Numerical investigation of the air-side thermal hydraulic performance of a louvered-fin and flat-tube heat exchanger at low reynolds numbers, Heat Transfer Engineering (2016) 1–45doi:10.1080/01457632.2016.1200382.

[9] D. Taler, J. Taler, Simple heat transfer correlations for turbulent tube flow, E3S Web of Conferences 13 (2017) 02008. doi:10.1051/e3sconf/20171302008.

[10] S. Eiamsa-ard, P. Promvonge, Experimental investigation of heat transfer and friction characteristics in a circular tube fitted with v-nozzle turbulators, International Communications in Heat and Mass Transfer 33 (5) (2006) 591–600. doi:https://doi.org/10.1016/j.icheatmasstransfer.2006.02.022.

[11] A. Habibi, B. Merci, G. Heynderickx, Impact of radiation models in cfd simulations of steam cracking furnaces, Computers & Chemical Engineering 31 (11) (2007) 1389 – 1406.

[12] M. Karim, J. Naser, Cfd modelling of combustion and associated emission of wet woody biomass in a 4 mw moving grate boiler, Fuel 222 (2018) 656–674.

[13] G. Tang, B. Wu, D. Bai, Y. Wang, R. Bodnar, C. Zhou, Cfd modeling and validation of a dynamic slab heating process in an industrial walking beam reheating furnace, Applied Thermal Engineering 132 (2018) 779–789.

[14] P. Tamadonfar, Ö. Gülder, Effects of mixture composition and turbulence intensity on flame front structure and burning velocities of premixed turbulent hydrocarbon/air bunsen flames, Combustion and Flame 162 (09 2015). doi:10.1016/j.combustflame.2015.08.009.

[15] A. Redko, R. Dzhyoiev, A. Davidenko, A. Pavlovskaya, S. Pavlovskiy, I. Redko, N. Kulikova, O. Redko, Aerodynamic processes and heat exchange in the furnace of a steam boiler with a secondary emitter, Alexandria Engineering Journal 58 (1) (2019) 89 – 101. doi:https://doi.org/10.1016/j.aej.2018.12.006.

[16] M. Manickam, M. Schwarz, J. Perry, Cfd modelling of waste heat recovery boiler, Applied Mathematical Modelling 22 (10) (1998) 823 – 840. doi:https://doi.org/10.1016/S0307-904X(98)10020-3.

[17] M. Tognoli, B. Najafi, F. Rinaldi, Dynamic modelling and optimal sizing of industrial fire-tube boilers for various demand profiles, Applied Thermal Engineering 132 (2018) 341–351.

[18] A. Abene, A. Rahmani, R. G. Seddiki, A. Moroncini, R. Guillaume, Heat transfer study in 3-pass fire-tube boiler during a cold start-up, Software Engineering 5 (4) (2018) 57.

[19] K. Sørensen, C. M. Karstensen, T. Condra, N. Houbak, Modelling and simulating fire tube boiler performance, in: Proceedings of SIMS, 2003, pp. 9–12.

[20] A. Bisetto, D. Del Col, M. Schievano, Fire tube heat generators: Experimental analysis and modeling, Applied Thermal Engineering 78 (2015) 236–247.

[21] F. G. Ortiz, Modeling of fire-tube boilers, Applied Thermal Engineering 31 (16) (2011) 3463–3478.

[22] M. Tognoli, B. Najafi, R. Marchesi, F. Rinaldi, Dynamic modelling, experimental validation, and thermo-economic analysis of industrial fire-tube boilers with stagnation point reverse flow combustor, Applied Thermal Engineering 149 (2019) 1394–1407.

[23] H. Hottel, A. Sarofim, Radiative transfer,(1967), New York 20–24.

[24] D. Taler, Simple power-type heat transfer correlations for turbulent pipe flow in tubes, Journal of Thermal Science 26 (4) (2017) 339–348.

[25] F. Dittus, L. Boelter, Heat transfer in automobile radiators of the tubular type, International Com-

munications in Heat and Mass Transfer 12 (1) (1985) 3 – 22. doi:https://doi.org/10.1016/0735-1933(85)90003-X.

[26] V. Gnielinski, Neue gleichungen für den wärme-und den stoffübergang in turbulent durchströmten rohren und kanälen, Forschung im Ingenieurwesen A 41 (1) (1975) 8–16.

[27] V. Gnielinski, New equations for heat and mass transfer in the turbulent flow in pipes and channels, STIA 41 (1) (1975) 8–16.

[28] W. Beyne, D. Daenens, B. Ameel, M. Van Belleghem, S. Lecompte, M. De Paepe, Steady state modeling of a fire tube boiler, in: 13th International Conference on Heat Transfer, Fluid Mechanics and Thermodynamics, 2017.

[29] P. Taylor, P. Foster, The total emissivities of luminous and non-luminous flames, International journal of Heat and Mass transfer 17 (12) (1974) 1591–1605.

[30] E. Talmor, Combustion hot spot analysis for fired process heaters, Gulf Pub Co, 1982.

[31] N. Lallemant, A. Sayre, R. Weber, Evaluation of emissivity correlations for h2o-co 2-n 2/air mixtures and coupling with solution methods of the radiative transfer equation, Progress in energy and combustion science 22 (6) (1996) 543–574.

[32] T. Smith, Z. Shen, J. Friedman, Evaluation of coefficients for the weighted sum of gray gases model (1982).

[33] C. F. Colebrook, C. M. White, Experiments with fluid friction in roughened pipes, Proceedings of the Royal Society of London. Series A-Mathematical and Physical Sciences 161 (906) (1937) 367–381.

[34] D. Brkić, New explicit correlations for turbulent flow friction factor (09 2017). doi:10.31219/osf.io/mazk2.

[35] M. Asker, O. Turgut, M. Coban, A review of non iterative friction factor correlations for the calculation of pressure drop in pipes, Journal of Science and Technology 4 (2014) 1–8. doi:10.17678/beujst.90203.

[36] L. Zeghadnia, J. L. Robert, B. Achour, Explicit solutions for turbulent flow friction factor: A review, assessment and approaches classification, Ain Shams Engineering Journal 10 (1) (2019) 243 – 252.

[37] X. Fang, Y. Xu, Z. Zhou, New correlations of single-phase friction factor for turbulent pipe flow and evaluation of existing single-phase friction factor correlations, Nuclear Engineering and Design 241 (3) (2011) 897 – 902, the International Conference on Structural Mechanics in Reactor Technology (SMiRT19) Special Section. doi:https://doi.org/10.1016/j.nucengdes.2010.12.019.

[38] J. Nikuradse, Strömungsgesetze in rauhen Rohren, VDI-Verlag, 1933.

[39] ICI Caldaie, https://www.icicaldaie.com/en.

[40] C. M. Fonseca, P. Fleming, An overview of evolutionary algorithms in multi objective optimization, Evolutionary Computation 3 (1995) 1–16.

[41] L. Pu, D. Qi, L. Xu, Y. Li, Optimization on the performance of ground heat exchangers for gshp using kriging model based on moga, Applied Thermal Engineering 118 (02 2017). doi:10.1016/j.applthermaleng.2017.02.114.

[42] F. Rinaldi, B. Najafi, Temperature measurement in wte boilers using suction pyrometers, Sensors 13 (11) (2013) 15633–15655. doi:10.3390/s131115633.

[43] S. Whitaker, Forced convection heat transfer correlations for flow in pipes, past flat plates, single cylinders, single spheres, and for flow in packed beds and tube bundles, AIChE Journal 18 (2) (1972) 361–371.

[44] F. White, Fluid mechanics/frank m. white (2003).

[45] F. Rinaldi, B. Najafi, Temperature measurement in wte boilers using suction pyrometers, Sensors 13 (11) (2013) 15633–15655.

[46] Fluent, Ansys 2020 R1 (2020).
URL `http://www.ansys.com/products/fluids/ansys-fluent`

[47] F. Menter, Two-equation eddy-viscosity turbulence models for engineering applications, AIAA Journal 32 (8) (1994) 1598–1605.

[48] E. H. Chui, G. D. Raithby, Computation of radiant heat transfer on a non orthogonal mesh using the finite-volume-method, Numerical Heat Transfer, Part B: Fundamentals 23 (3) (1993) 269–288.

[49] W. A. Fiveland, Three-dimensional radiative heat-transfer solutions by the discrete-ordinates method,

AIAA J. Thermophysics 2 (4) (1988) 309–316.
[50] Species transport equations.
URL https://www.afs.enea.it/project/neptunius/docs/fluent/html/th/node128.htm
[51] Y. Cengel, T. M. Heat, A practical approach, Mc-Graw Hill Education, Columbus, GA, USA, 2003.
[52] D. W. G. R. H. Perry, Perry's Chemical Engineers' Handbook, 2007.
[53] J. Franke, W. Frank, Application of generalized richardson extrapolation to the computation of the flow across an asymmetric street intersection, Journal of Wind Engineering and Industrial Aerodynamics 96 (10) (2008) 1616–1628, 4th International Symposium on Computational Wind Engineering (CWE2006). doi:https://doi.org/10.1016/j.jweia.2008.02.003.
URL https://www.sciencedirect.com/science/article/pii/S0167610508000342
[54] I. H. Bell, J. Wronski, S. Quoilin, V. Lemort, Pure and pseudo-pure fluid thermophysical property evaluation and the open-source thermophysical property library coolprop, Industrial & Engineering Chemistry Research 53 (6) (2014) 2498–2508.
[55] E. N. Sieder, G. E. Tate, Heat transfer and pressure drop of liquids in tubes, Industrial & Engineering Chemistry 28 (12) (1936) 1429–1435.
[56] G. Filonienko, Friction factor for turbulent pipe flow, Teploenergetika 1 (4) (1954) 40–44.
[57] G. Brown, The darcy-weisbach equation, Oklahoma State University–Stillwater (2000).
[58] B. Petukhov, T. Irvine, J. Hartnett, Advances in heat transfer, Academic, New York 6 (1970) 503–564.
[59] J. Blank, K. Deb, Pymoo: Multi-objective optimization in python, IEEE Access 8 (2020) 89497–89509.
[60] T. Selleri, B. Najafi, F. Rinaldi, G. Colombo, Mathematical modeling and multi-objective optimization of a mini-channel heat exchanger via genetic algorithm, Journal of Thermal Science and Engineering Applications 5 (3) (2013).
[61] B. Najafi, H. Najafi, M. Idalik, Computational fluid dynamics investigation and multi-objective optimization of an engine air-cooling system using genetic algorithm, Proceedings of the Institution of Mechanical Engineers, Part C: Journal of Mechanical Engineering Science 225 (6) (2011) 1389–1398.
[62] K. Deb, A. Pratap, S. Agarwal, T. Meyarivan, A fast and elitist multiobjective genetic algorithm: Nsga-ii, IEEE transactions on evolutionary computation 6 (2) (2002) 182–197.
[63] J. Blank, K. Deb, A running performance metric and termination criterion for evaluating evolutionary multi-and many-objective optimization algorithms, in: Proc. IEEE World Congr. Comput. Intell.(WCCI), 2020.

View publication stats